Fast Central Catadioptric Line Extraction

Jean Charles Bazin, Cédric Demonceaux, Pascal Vasseur

Fast Central Catadioptric Line Extraction

Jean Charles Bazin[1], Cédric Demonceaux[2], and Pascal Vasseur[2]

[1] Korea Advanced Institute of Science and Technology, KAIST
[2] CREA-EA3299- University of Picardie Jules Verne, France
JeanCharles.Bazin@gmail.com
{Cedric.Demonceaux,Pascal.Vasseur}@u-picardie.fr

Abstract. Lines are particularly important features for different tasks such as calibration, structure from motion, 3D reconstruction in computer vision. However, line detection in catadioptric images is not trivial because the projection of a 3D line is a conic eventually degenerated. If the sensor is calibrated, it has been already demonstrated that each conic can be described by two parameters. In this way, some methods based on the adaptation of conventional line detection methods have been proposed. However, most of these methods suffer from the same disadvantages than in the perspective case (computing time, accuracy, robustness, ...). In this paper, we then propose a new method for line detection in central catadioptric image comparable to the polygonal approximation approach. With this method, only two points of a chain allows to extract with a very high accuracy a catadioptric line. Moreover, this algorithm is particularly fast and is applicable in realtime. We also present experimental results with some quantitative and qualitative evaluations in order to show the quality of the results and the perspectives of this method.

1 Introduction

Catadioptric vision sensors (associations of a camera with a mirror) are now broadly used in many applications such as robot navigation, 3D scene reconstruction or video surveillance [1]. Their large field of view is indubitably the major reason of this success. Baker and Nayer classified these sensors in two respective categories [2]. First, sensors with a single viewpoint, named central catadioptric sensors are made of parabolic mirror associated to orthographic camera and hyperbolic, elliptic and plane mirrors with perspective camera. The second category with different viewpoints has geometric properties less significant and is made of the other possibilities of association between mirrors and cameras. In this paper, we are only interested in central sensors which permit a geometrically correct reconstruction of the perspective image from the original catadioptric image. However, their employment presents some drawbacks because of the deformations induced by the mirror. For example, some very useful classical treatments in perspective image processing can be no more performed on catadioptric images because they are inadequate. One of these major treatments deals with line extraction. Thus, while in the perspective case line detection is perfectly known and efficiently solved, with catadioptric images the

problem is absolutely not trivial. Indeed, the projection of any 3D real line is a conic eventually degenerate. Thus, in the case of an uncalibrated sensor, it is necessary to estimate five parameters for each line while only two parameters are sufficient for a calibrated sensor. If we consider the projection of a 3D point by the way of the unitary sphere (fig. 1(a)) as proposed in [3] [4] [5] with the formalism defined in [3] [4], we can define oriented projective ray P_1 passing by 3D point x_w and the center of the sphere. This ray intersects the surface of the sphere in x_s. We then consider oriented projective ray P_2 passing by x_s and a point situated on the z-axis between the center of the sphere and the north pole. This point is at distance ξ from the center of the sphere and depends only on the mirror geometric characteristics. P_2 intersects plane at infinity in point x_i. Finally, homography H defined between the plane at infinity and the catadioptric image plane projects point x_i into point x_c. H includes intrinsic parameters of the camera, possible rotations between the sphere frame and the camera frame, and finally the parameters of the mirror. According to this model, we can develop the projection of a 3D line into the catadioptric image plane (fig. 1(b)). We consider plane Π_R which contains the real 3D line and the center of the sphere. This plane intersects the sphere and then defines a great circle onto its surface. The set of oriented projective rays passing by the points of the great circle and point O_2 define then a cone which intersects plane at infinity into conic C_i. Finally, homography H transforms C_i into conic C_c in the catadioptric image plane. In plane at infinity, we know that the equation of conic C_i is equal to :

$$C_i = \begin{bmatrix} n_x^2(1-\xi^2) - n_z^2\xi^2 & n_x n_y(1-\xi^2) & n_x n_z \\ n_x n_y(1-\xi^2) & n_y^2(1-\xi^2) - n_z^2\xi^2 & n_y n_z \\ n_x n_z & n_y n_z & n_z^2 \end{bmatrix} \qquad (1)$$

with $(n_x, n_y, n_z)^T$ the vector which describes the normal to plane P_w which contains the 3D line. We obtain the equation of conic C_c in image plane thanks to the following relation :

$$C_c = H^{-T} C_i H^{-1} \qquad (2)$$

Finally, a pixel $x_c = (u \quad v \quad 1)^T$ belongs to the conic C_c if the equality $x_c^T C_c x_c = 0$ is verified.

In this paper, we propose a new method for calibrated catadioptric line detection which permits a very fast, robust and accurate detection. The proposed approach consists in roughly estimating the possible catadioptric lines in the image and in verifying if each possible line is a real catadioptric line. The rest of the paper is organized as follows. Section II is devoted to the related works which deal with catadioptric line detection in calibrated and uncalibrated cases. In section III, we present a complete description of the algorithm. Section IV is devoted to experimental results with quantitative and qualitative evaluations. We finally conclude in section V on different perspectives.

2   Related Works

The methods of catadioptric line detection and estimation can be divided in three categories. The first class deals with methods applicable as well in the calibrated case as in the uncalibrated case and includes the algorithms of conic fitting
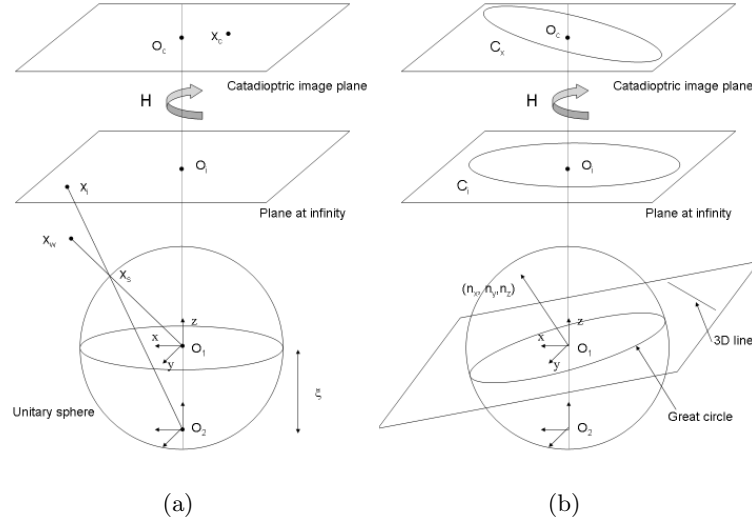
Fig. 1. (a) Image formation model. Example of projection via the unitary sphere for a 3D point. (b) Projection of a 3D line via the unitary sphere into the catadioptric image plane.

[6]. The second category concerns calibrated sensors and most of the proposed techniques in this category are based on adaptation of Hough transform [7] [8] [9]. Methods for uncalibrated sensors form the third category. These methods use particular geometric constraints of catadioptric sensors and are generally dedicated to paracatadioptric sensors [10] [11]. In the rest of this section, we only develop the two first categories because the third is not enough general and concerns only paracatadioptric cameras.

Conic fitting algorithms determine the curve that best fits the data points according to a certain distance metric [6]. In [10], the authors present a comparison of the normal least squares (LMS), approximate mean square (AMS), Fitzgibbon and Fisher (FF) [12], gradient weighted least square fitting (GRAD) and orthogonal distances (ORTHO) methods for the specific problem of paracatadioptric line detection. Their conclusions are that GRAD and ORTHO are the most robust to noise and that all methods perform poorly when the amplitude of the occlusion is above 240°. Since most of the catadioptric lines have an amplitude less than 45°, it appears clearly that these methods are unsuitable for general central catadioptric line detection and estimation. Moreover, these methods suppose that the pixels from the edges have been already classified into chains representing the different possible catadioptric lines.

In the calibrated case, homography H and parameter ξ are known. In this way, a 3D line is determined thanks to a vector $(n_x, n_y, n_z)^T$. This vector represents the normal of the great circle on the unitary sphere obtained by the

intersection of the plane which contains the center of the sphere and the 3D real line (fig. 1(b)). A 3D real line can be also represented by two angles ϕ and θ which respectively are the elevation angle and the azimuth angle of the normal vector. Each catadioptric line is then represented by only two parameters and a simple adaptation of the Hough transform can solved the problem. This is this kind of approach which is proposed in [8] and [7]. The mean difference between these methods deals with the space in which the treatments are performed. In [7], the image is projected on the unitary sphere and the 3D coordinates of the pixels are then used while in [8], they apply the algorithm directly in the image. Although these two approaches present interesting results, it is worth noting that they present the classic defects of the Hough transform such as the best sampling step for ϕ and θ for example. In order to avoid these drawbacks, we can note that if two pixels of a catadioptric line are known, it is then possible to compute the normal of the great circle and then to obtain the corresponding values of ϕ and θ. In [9], the authors propose a randomized Hough transform which selects randomly two points in the image of edges in order to compute the ϕ and θ angles. These angles are then used in an accumulator for the detection of the most confident catadioptric lines.

3   Central Catadioptric Line Detection Algorithm

Our line detection algorithm for central catadioptric sensor consists first in applying a Canny edge detector (Fig 4(b)). Then, we proceed to an edge chaining which consists in extracting connected pixels from edges in order to form lists with a length superior or equal to a threshold (NbPixels) (Fig 4(c)). To detect the lines in the scene consists then in verifying if these chains are the projections of 3D lines. In this way, we apply a split and merge algorithm of the chains. First, an adaptation of the polygonal approximation of the classical perspective case is proposed in order to find which chains or parts of chains are catadioptric projections of lines. This process is performed thanks to a division criterion which cuts the chains at a particular position if the chain is not verified as a catadioptric line. Next, we use a fusion criterion in order to group the different chains in the image which represents the same central catadioptric lines. These both criteria are discussed in the following of the paper.

3.1   Division Criterion

Consider the two endpoints of a chain of N pixels with coordinates $P_1 = (X_1, Y_1, Z_1)$ and $P_2 = (X_2, Y_2, Z_2)$ on the unitary sphere S^2. These points define a single central catadioptric line in the image and then a great circle $\mathcal{C}$ on the sphere (cf fig(1(a)(b)). This circle results from the intersection of the unitary sphere and a plane which contains the sphere origin 0_1 and whose a normal vector is $\overrightarrow{n} = \overrightarrow{O_1P_1} \times \overrightarrow{O_1P_2} = (n_x, n_y, n_z)^T$. Then, the equation of $\mathcal{C}$ is :

$$\begin{cases} n_x X + n_y Y + n_z Z = 0 \\ (X, Y, Z) \in S^2 \end{cases}$$

We consider that a point on the sphere with coordinates (X_i, Y_i, Z_i) of the chain belongs to the great circle if the distance between this point and the plane defined by the great circle is less than a threshold:

$$|n_x X_i + n_y Y_i + n_z Z_i| \leq \text{DivThreshold}.$$

This chain is then considered as a central catadioptric line if at least 95% of its points belong to the great circle.

In the opposite case, we cut the chain into two sub-chains at the point (X_j, Y_j, Z_j) which maximizes the following error $||(X_i, Y_i, Z_i).\overrightarrow{n}||$, $i = 1 \cdots n$ (the furthest point from the plane).

This division step stops when the chain is considered as a central catadioptric line or when the length of the sub-chains is less than the threshold (NbPixels). At the end of this step, we then obtain the whole set of central catadioptric lines in the image. However this method may generate a multi-detection of the same lines. In order to compensate this drawback, we then propose to merge the similar catadioptric lines.

3.2 Fusion Criterion

Let define two catadioptric lines d_1 and d_2 detected with the previous method. These lines respectively characterized by $\overrightarrow{n_1}$ and $\overrightarrow{n_2}$ define two planes in the 3D space passing through the origin of the unitary sphere, $\Pi_1 = \{U = (X, Y, Z) \in \mathbb{R}^3, \overrightarrow{n}_1.U = 0\}$ and $\Pi_2 = \{U = (X, Y, Z) \in \mathbb{R}^3, \overrightarrow{n}_2.U = 0\}$. We consider that these detected catadioptric lines are similar if they define the same 3D plane, that is to say if :

$$1 - |\overrightarrow{n}_1.\overrightarrow{n}_2| \leq \text{FusThreshold}.$$

In this case, the two catadioptric lines are merged into a single line. The catadioptric line equation is then updated from the pixels of the chains which belong to d_1 and d_2 as follows. Let note respectively $M^1 = (X_i^1, Y_i^1, Z_i^1)_{i=1 \cdots N_1}$ and $M^2 = (X_i^2, Y_i^2, Z_i^2)_{i=1 \cdots N_2}$, the pixels of catadioptric line d_1 (resp. d_2). Let M, the matrix of dimension $(N_1 + N_2) \times 3$,

$$M = \begin{pmatrix} X_1^1 & Y_1^1 & Z_1^1 \\ \vdots & \vdots & \vdots \\ X_{N_1}^1 & Y_{N_1}^1 & Z_{N_1}^1 \\ X_1^2 & Y_1^2 & Z_1^2 \\ \vdots & \vdots & \vdots \\ X_{N_2}^2 & Y_{N_2}^2 & Z_{N_2}^2 \end{pmatrix},$$

The normal vector $\overrightarrow{n} = (n_x, n_y, n_z)^T$ of the great circle associated to the catadioptric line is then solution of :

$$M.\overrightarrow{n} = (0, \cdots, 0)^T. \tag{3}$$

The solution of (3) is obtained from the SVD of matrix M [13].

4 Experimentations

We have tested our central catadioptric line detector on different kinds of omnidirectional images. We first propose some results with synthesis images for which we perfectly know the line equations in order to show the accuracy of the approach. Then, some results on real images are also proposed. In the whole set of experimentations except in one indicated case, the different thresholds are fixed as follows : NbPixels =100, DivThreshold = 0.0005, FusThreshold = 1°.

4.1 Synthesis Images

We have generated two synthesis images for which we perfectly know the calibration parameters and line equations. The first image contains five catadioptric lines (fig 2(a)). The five lines are obviously easily detected (fig 2(b)). However, results show a very high accuracy of the catadioptric line estimation. Indeed, contrary to Hough based methods which require a sampling of the search space and for which the accuracy depends on this sampling, in the proposed method the catadioptric line estimation is performed analytically. Thus, let note H_c^i the 3×3 matrix of the conic associated to a catadioptric line i ($i = 1 \cdots 5$) and $\widehat{H_c^i}$, the estimation of this matrix from the proposed method. For the five catadioptric lines of the first image Fig 2(a), the mean error :

$$\frac{1}{5} \sum_{i=1}^{5} \frac{||H_c^i/H_c^i(3,3) - \widehat{H_c^i}/\widehat{H_c^i}(3,3)||}{||H_c^i||} = 5.10^{-5}.$$

$$(a) \qquad\qquad\qquad (b)$$
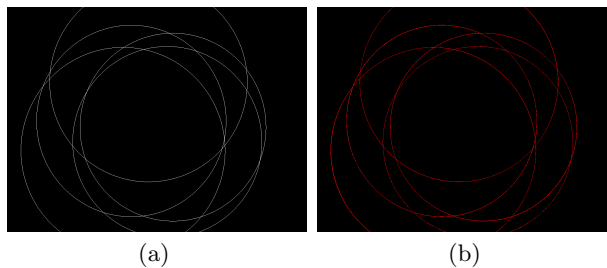
Fig. 2. (a)Original image, (b) Detected catadioptric lines.

The second synthesis image is composed of eight catadioptric lines and two 'false' catadioptric lines (fig 3(a)). Results show that the eight catadioptric lines are correctly detected Les résultats montrent bien que les 8 droites sont correctement détectées while the two ellipses which are 'false' catadioptric lines are not detected (fig 3(b)). Nevertheless, if the minimal length NbPixel decreases (in this example, NbPixel=50), we can note that some parts of these ellipses may correspond to catadioptric lines (fig 3(c)).
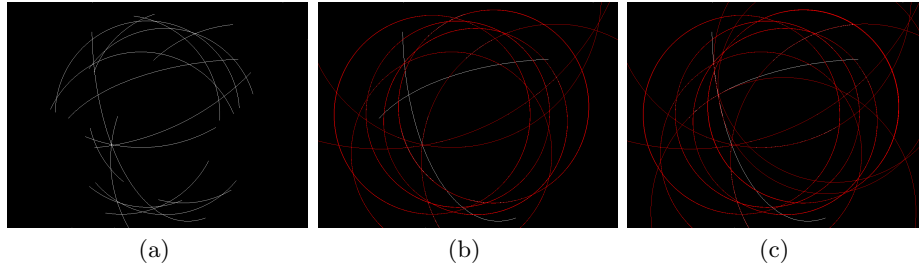
Fig. 3. (a)Original image, (b) Red catadioptric lines correspond to detected catadioptric lines, (c) False catadioptric lines whan the length NbPixel is too low.

4.2   Real Catadioptric Images

We present here result for a real catadioptric image. In this case, sensor has been calibrated with the method described in [4]. This image (fig 4(a)) is a paracatadioptric image issued from the calibration toolbox proposed by Barreto [4]. In figure 4(b), we present the result of Canny edge detector and consecutively the detected chains of pixels extracted for the catadioptric line verification (fig 4(c)). Figure 4(d) shows the catadioptric line detection before the fusion step while figure 4(e) presents the final result after the fusion step. In figure 4(f), we propose a more detailed view of a part of the image in order to show the accuracy of the results. Finally, from a computational time point of view, the method takes near 3 seconds with Matlab. A real time implementation constitutes the next perspective of this work.

5   Conclusion

In this paper, we deal with the problem of line detection in central catadioptric images. Our method is valid for calibrated sensor and is comparable to the polygonal approximation algorithm. Indeed, it consists in looking for pixels in chains of edges which correspond to catadioptric lines thanks to an analytic approach contrary to previous methods based on Hough transform which depends on the sampling of the search space. Moreover, we then obtain a very fast algorithm which could be implemented for real time applications.

References

1. Benosman, R., Kang, S.B.: Panoramic Vision: Sensors, Theory, Applications. Springer (2001)
2. Baker, S., Nayar, S.K.: A theory of single-viewpoint catadioptric image formation. International Journal on Computer Vision **35**(2) (1999) 175–196

(a)   (b)   (c)

(d)   (e)   (f)
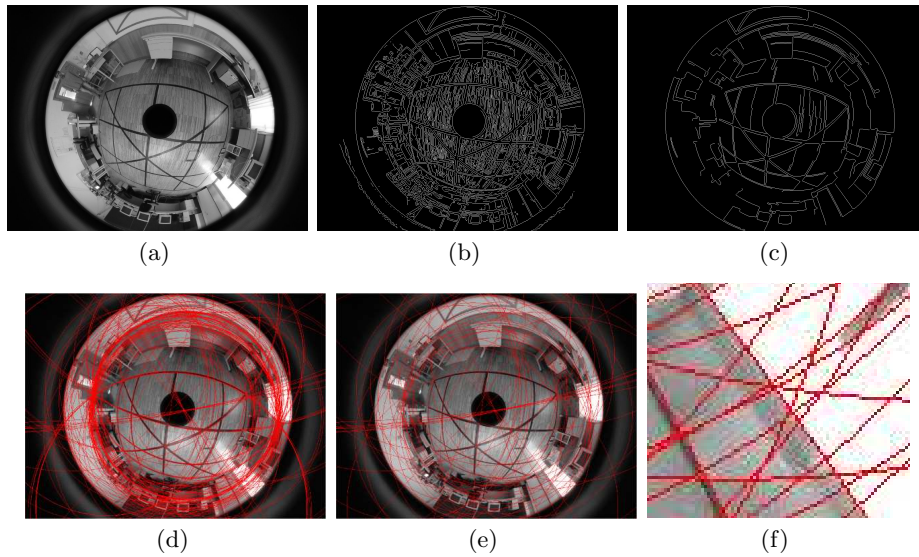
Fig. 4. (a)Original image, (b) Canny edge detector result, (c) Extracted chains, (d) Catadioptric line detection results after division step, (e) Catadioptric line detection results after fusion step, (f) Detailed view of final results.

3. Barreto, J.P., Araújo, H.: Geometric properties of central catadioptric line images. In Heyden, A., Sparr, G., Nielsen, M., Johansen, P., eds.: ECCV (4). Volume 2353 of Lecture Notes in Computer Science., Springer (2002) 237–251
4. Barreto, J.P.: General Central Projection Systems: Modeling, Calibration and Visual Servoing. PhD Thesis, University of Coimbra (2003)
5. Geyer, C., Daniilidis, K.: Catadioptric projective geometry. International Journal of Computer Vision **45**(3) (2001) 223–243
6. Zhang, Z.: Parameter estimation techniques: a tutorial with application to conic fitting. Image Vision Comput. **15**(1) (1997) 59–76
7. Vasseur, P., Mouaddib, E.M.: Central catadioptric line detection. In: BMVC04. (2004) xx–yy
8. Ying, X., Hu, Z.: Catadioptric line features detection using hough transform. In: ICPR (4), IEEE Computer Society (2004) 839–842
9. Mei, C., Malis, E.: Fast central catadioptric line extraction, estimation, tracking and structure from motion. In: IROS. (2006)
10. Barreto, J.P., Araújo, H.: Fitting conics to paracatadioptric projections of lines. Computer Vision and Image Understanding **101**(3) (2006) 151–165
11. Vandeportaele, B., Cattoen, M., Marthon, P.: A fast detector of line images acquired by an uncalibrated paracatadioptric camera. In: ICPR (3), IEEE Computer Society (2006) 1042–1045
12. Fitzgibbon, A.W., Fisher, R.B.: A buyer's guide to conic fitting. In: BMVC95. (1995)
13. Jennings, A., McKeown, J.J.: Matrix Computation. 2 edn. John Wiley & Sons (1992)